Chemical Science

ROYAL SOCIETY OF CHEMISTRY

EDGE ARTICLE

View Article Online
View Journal | View Issue

Cite this: *Chem. Sci.*, 2023, **14**, 5503

All publication charges for this article have been paid for by the Royal Society of Chemistry

Received 1st February 2023
Accepted 19th April 2023

DOI: 10.1039/d3sc00563a

rsc.li/chemical-science

Orthometric multicolor encoded hybridization chain reaction amplifiers for multiplexed microRNA profiling in living cells†

Wei Wei,[abc] Yiyi Zhang,[b] Fan Yang,[b] Liping Zhou,[b] Yufan Zhang,[ab] Yeyu Wang,[abc] Shuangshuang Yang,[ab] Jinze Li[ab] and Haifeng Dong *[ab]

Multiplexed microRNA (miRNA) profiling of more than four types in living cells is challenging due to fluorescent spectral overlap, representing a significant limitation in studying the complex interactions related to the occurrence and development of diseases. Herein, we report a multiplexed fluorescent imaging strategy based on an orthometric multicolor encoded hybridization chain reaction amplifier named multi-HCR. The targeting miRNA can trigger this multi-HCR strategy due to the specific sequence recognition, and then its self-assembly to amplify the programmability signals. We take the four-colored chain amplifiers, showing that the multi-HCR can form 15 combinations simultaneously. In a living process of hypoxia-induced apoptosis and autophagy under complicated mitochondria and endoplasmic reticulum stress, the multi-HCR demonstrates excellent performance in detecting eight different miRNA changes. The multi-HCR provides a robust strategy for simultaneously profiling multiplexed miRNA biomarkers in studying complicated cellular processes.

Introduction

Living cells are the most precise molecular machines, integrating internal gene networks with external cellular behavior in response to multiple stimuli.[1] High multiplexing fluorescence (FL) imaging capability is crucial for studying the interacting regulatory elements in a biological system's developmental and pathological processes.[2] However, performing parallel mapping of multiple interactions is challenging owing to the emission spectral overlap.[3] MicroRNAs (miRNAs) are novel biomarkers for multiple diseases, including cancers and neurodegenerative and cardiovascular diseases.[4] They are 18–22 nucleotide endogenous non-coding RNAs that govern the expression of target genes by recruiting the RNA-induced silencing complex to the specific sequences at the 3′-UTR of target mRNAs and disrupting the stability of mRNA.[5] The great clinical potential of miRNAs for recognizing typical disease signatures depends mainly upon the ability to parallelly map the expression profile and concentration changes of multiple miRNAs.[2a,6]

Over the past few decades, *in situ* fluorescent hybridization has been an indispensable tool for studying genetic regulation in a morphological context.[7] Current multiplexed methods, such as the rolling circle amplification (RCA),[3b] Exchange-Points Accumulation in Nanoscale Topography technique (Exchange-PAINT),[8] sequential hybridization[9] and split-probe strategy with multiplexed fluorescence *in situ* hybridization (split-FISH),[10] require serial amplification with enzyme-dependent performance, limiting their use to fixed cells. In contrast, enzyme-free amplification techniques such as hybridization chain reaction (HCR) and catalyzed hairpin amplification (CHA) are more suitable for living cell detection. Significantly, the limit of detection of HCR-based miRNA imaging in living cells can be down to attomole (aM) levels,[11] satisfying the high sensitivity requirement of intracellular miRNA (picomolar (pM)–femtomolar (fM) range) analysis.[2a,12] Our group also previously developed several HCR strategies for miRNA imaging;[13] however, owing to the spectral overlap between fluorophores,[3a] simultaneously mapping more than four different miRNAs in living cells is challenging.

Herein, we developed an orthometric multicolor encoded hybridization chain HCR amplifier (multi-HCR) to implement 15 combinations for simultaneously mapping miRNAs in living cells. The multi-HCR consists of metastable nucleic acid hairpins (H) modified with four kinds of fluorophores (Alexa Fluor (AF) 405, AF488, AF594, and AF647). The fluorescent hairpins were separately modified on a biodegradable mesoporous silica

[a]*Marshall Laboratory of Biomedical Engineering, Shenzhen Key Laboratory for Nano-Biosensing Technology, School of Biomedical Engineering, Shenzhen University Medical School, Shenzhen University, 518060, Guangdong, China. E-mail: hfdong@szu.edu.cn*

[b]*Beijing Key Laboratory for Bioengineering and Sensing Technology, School of Chemistry and Bioengineering, University of Science and Technology Beijing, 30 Xueyuan Road, 100083, Beijing, China*

[c]*Beijing Yaogen Biotechnology Co. Ltd, 26 Yongwangxi Road, 102609, Beijing, China*

† Electronic supplementary information (ESI) available: Binding specificity and stability analysis, electron microscopy observation, multi-HCR analysis details, fluorescent composition masses and probe sequences. See DOI: https://doi.org/10.1039/d3sc00563a

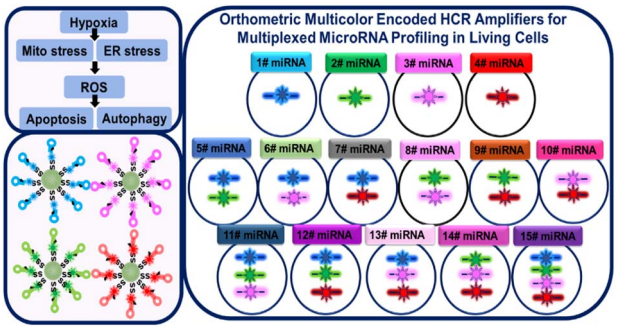

Scheme 1 Schematic presentation of orthometric multi-HCR amplifiers for multiplexed miRNAs profile in living cells.

nanoparticles (DMSN) vector, forming a spherical structure of DMSN@H. The DMSN vector endows the hairpins with high cell penetration ability.[14] After cellular uptake, the endogenous glutathione (GSH) decomposes DMSN to release the hairpins.[15] Target miRNAs complementary to the hairpin probes trigger HCR and self-assemble into encoded tethered fluorescent amplifiers. Owing to the sequence-specific and ordered-dye designation, these hairpins can be self-assembled in an orthometric way to simultaneously achieve 15 combinations for miRNA imaging in a colorectal cancer cell model (Scheme 1). Excellent performance was realized when imaging eight different miRNAs under hypoxia-induced mitochondria (Mito) stress and endoplasmic reticulum (ER) stress cross-talking in related reactive oxygen species (ROS), apoptosis, and autophagy pathways.

Results and discussion

HCR orthometric assembly feasibility analysis. Inspired by the logical combination of FL signals,[6a,16] the HCR extension hairpin chains containing different FL dyes were designed to programmatically self-assemble and be recognized in an orthometric combination manner during the HCR reaction procedure (Fig. S1†). To test this hypothesis, a series of tests for miRNA-155-triggered FL hairpins with similar self-dimer structures were designed (Fig. S2 and Table S1†). According to the base complementarity reaction law and the principle of the classical HCR reaction, the introduction of an initiator strand (target miRNA) triggers a chain reaction of alternating kinetic escapes by the two hairpin species corresponding to "polymerization" into a nicked double helix, then amplification of the initiator recognition event continues until the supply of H1 or H2 is exhausted, forming DNA polymers,[17] as depicted by transmission electron microscopy (TEM) (Fig. 1a and S3†). Native polyacrylamide gel electrophoresis (native-PAGE) demonstrated the excellent specificity of the HCR assembly (Fig. S4†). FL analysis using AF488-labeled miR-155 probes showed its excellent base-mismatch discrimination ability (Fig. 1b), and it could respond in a target concentration-dependent manner (Fig. S5†). In principle, using three fluorescent-dye (AF488, AF594, AF647)-labeled hairpin structures, it could be orthogonally self-assembled into seven different encoded amplifiers through the equation of $N = C_3^1 +$

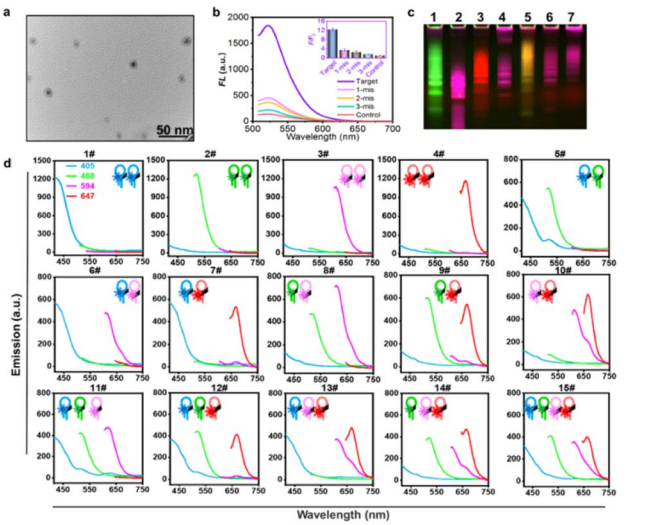

Fig. 1 Feasibility analysis of the multi-HCR assembly. (a) Representative TEM images for HCR self-assembled amplifier. (b) Base-mismatched analysis toward the complementary target (miRNA-155, 100 nM). Single-base-mismatched strand (1 mis, 100 nM); two-base-mismatched strand (2 mis, 100 nM), three-base-mismatched strand (3 mis, 100 nM), and control (PBS). (c) Fluorescent native-PAGE electrophoresis (2 μM) of three-color multi-HCR encoded amplifiers. (d) FL emission spectra of self-assembled encoded amplifiers from four different dye-labeled hairpins in response to target miRNA-155. Each experiment was repeated three times.

$C_3^2 + C_3^3$; $N = 7$ (Fig. 1c and S6†). Accordingly, four different fluorescent-dye (AF405, AF488, AF594, AF647)-labeled hairpin structures could be self-assembled into 15 kinds of encoded amplifiers ($N = C_4^1 + C_4^2 + C_4^3 + C_4^4$; $N = 15$) with distinct FL spectra (Fig. 1d, S7, S8 and Table S2†), which holds great potential for multiplexed miRNA profiling. Although there was Förster Resonance Energy Transfer (FRET) in the adjacent dyes, its effect was weak; it could not entirely disappear a color;[3b,18] the FRET had a limited effect on the classification ability of the multi-HCR system (Fig. 1d). This highlights the novelty of the multi-HCR system in that its multiplexed coding capability comes from the color combinations, not intensity, which makes it an easy-to-operate tool for multiple miRNA profiling.

GSH response and target miRNA-triggered multi-HCR in living cells

As the primary intracellular antioxidant inside cells, GSH plays a critical role in mammalian cell function. It was reported that the GSH concentration inside the cells is about 1×10^{-3}–10×10^{-3} M,[19] as compared with 2×10^{-6}–40×10^{-6} M in blood and other body fluids.[20] What is more, cancer cells have about four-fold higher GSH than normal cells,[21] indicating that GSH could also be used as an effective signal molecule for enhancing the specificity of tumor detection. On the other hand, to improve the cellular transfection efficiency of the DNA hairpin probes,[14a,22] we modified the HCR hairpins on biodegradable DMSN by a disulfide bond,[23] forming spherical nucleic acid structures of DMSN@H, termed multi-HCR (Fig. 2a), which has been reported to possess high stability, excellent

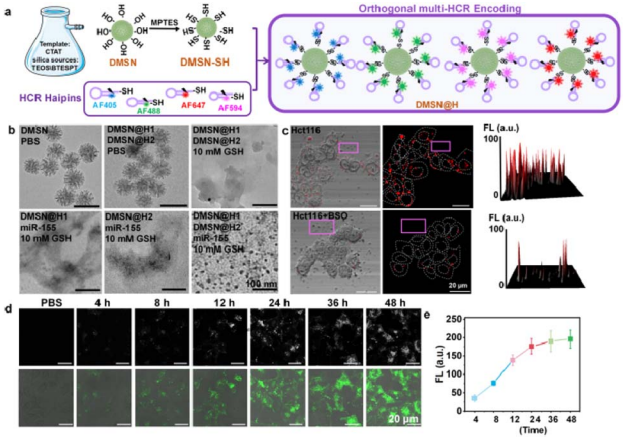

Fig. 2 GSH-activated and miRNA target-triggered multi-HCR barcode. (a) Assembly process diagram for multi-HCR. (b) Representative TEM of DMSN@H after 24 h treatment in different conditions. (c) Representative CLSM images of the multi-HCR-treated Hct116 cells with or without GSH inhibitor, BSO. The 3D FL intensity surface profiling pictures were acquired by ImageJ software (version 1.52i, USA). (d) Representative CLSM images and (e) mean FL intensity of the multi-HCR-treated cells at different incubation times. Each experiment was repeated three times.

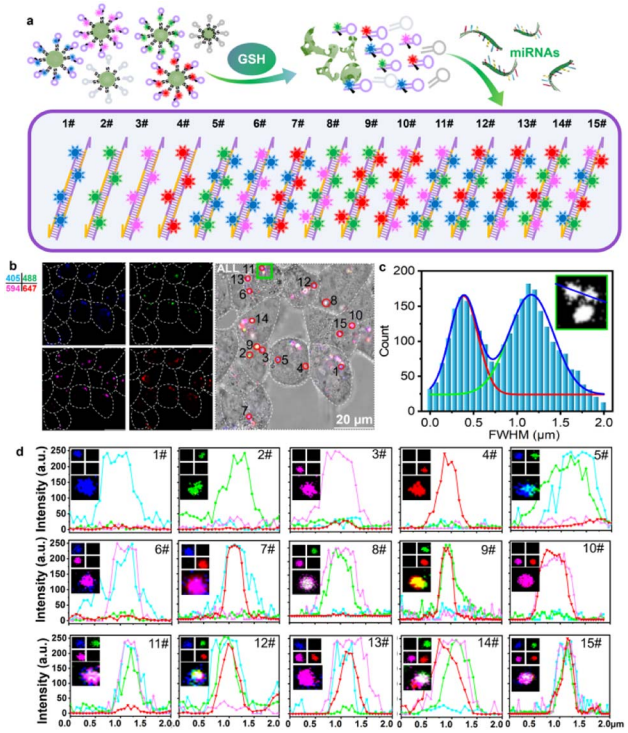

Fig. 3 Multi-HCR encoded in living cells. (a) Illustration of the multi-HCR barcode encoded in living cells. (b) Representative CLSM images for the four-color DMSN@H simultaneously encoded in living cells. (c) Gaussian curve analysis of the adjacent FL dots in the green box of (b). (d) Representative images and FL curves of the 15 kinds of barcodes. Each experiment was repeated three times.

biocompatibility, and high cell entry ability.[24] The loading efficiency for the hairpins was calculated to be 48%. The TEM results in Fig. 2b show that under the stimulation of 10 mM GSH, the DMSN vectors were degraded and the hairpins were released from the DMSN vectors, and the co-existing H1 and H2 were self-assembled into spherical DNA gel amplifiers in the presence of target miRNA, confirming that the DMSN@H was activated in a GSH-responsive manner. The Cell-Counting-Kit-8 (CCK-8) test verified good biosafety for living colon cancer cells (Hct116) (Fig. S9†), which is very important for nanoparticle probes to be used in living cell imaging. Confocal laser scanning microscopy (CLSM) analysis confirmed that the DMSN@H had no FL (purple box) unless it had entered the cells (Fig. 2c). Notably, when the Hct116 cells were pretreated with GSH inhibitor L-buthionine sulfoximine (BSO),[23c] the mean FL intensity decreased dramatically (~5.4 fold), further verifying the GSH-mediated release of hairpins probes, which provided endogenous GSH-activatable and spatially controllable miRNA imaging. Moreover, the FL intensity was observed to increase with the reaction time, and it reached a plateau after 24 h incubation with the cells (Fig. 2d and e). The AF488-labeled DMSN@H barcodes toward miRNA-155 were put in pH 7.2, pH 6.0, and pH 5.0 cell culture mediums for 4 h. The size and FL intensity were measured, as shown in Fig. S10;† the results show that the sizes and FL were stable under different pH. These results strongly confirmed the GSH-responsive and target miRNA-triggered self-assembly-encoded process of DMSN@H barcodes in living tumor cells.

The encoding ability of multi-HCR amplifiers in living cells

We further tested the intracellular encoding ability of the multi-HCR system. As illustrated in Fig. 3a, the intracellular DMSN@H decomposed in response to endogenous GSH and released the hairpins loaded with different color dyes. The presence of the target miRNA initiated the cross-opening of two specific DNA hairpins, yielding double helices that are analogous to alternating copolymers, and different colored dyes were enclosed into the barcode for classification. As shown in Fig. 3b, DMSN@H (Table S3†) was mixed and treated with the living Hct116 cells for intracellular miRNA-155 imaging. The encoding composition could be acquired by CLSM sequencing scanning the four FL channels with an appropriate exciting laser and emission filter. In Fig. 3c, Gaussian curve analysis of the full width at half maximum (FWHM) of two adjacent dots in the green box of Fig. 3b showed that the multi-HCR barcodes could be well distinguished using the CLSM system. The 15 different kinds of amplifiers with distinct emission characteristics were detected synchronously. The dot analysis shown in Fig. 3d verified that the multi-HCR approach is a simple way to distinguish miRNA types based on the encoded color composition but not based on the intensity. These demonstrated the excellent encoding ability of multi-HCR for *in situ* multiplexed miRNA analysis.

Multiplexed miRNA profiling under hypoxia-induced Mito/ER stress and apoptosis/autophagy processes

Finally, we attempted to simultaneously detect multiple miRNAs that vary during hypoxia-induced Mito/ER stress processes

and apoptosis/autophagy responses. Hypoxia can induce Mito and ER stress, leading to apoptosis and autophagy in living cells. As critical regulators, miRNA expression alters in response to the hypoxia to influence downstream cellular functions involved in apoptosis and autophagy.[25] Hypoxia adaptation is essential for cancer cell progression; however, little research has investigated the changes in multiplexed miRNA profiles in hypoxia-induced Mito/ER stress and apoptosis/autophagy. First, hypoxia-induced Mito–ER stress and apoptosis/autophagy experiments were performed to prove the elaborate cell behavior alterations in the hypoxic microenvironment (Fig. S11†). Then, we attempted to simultaneously monitor eight reported hypoxic-responsive miRNAs in living cancer cells using the orthogonal multi-HCR strategy (Fig. 4a and Table S4†). Different multi-HCR chains for eight types of miRNAs involved in these processes[26] were designed to map multiplexed miRNAs (Fig. S12, S13 and Table S5†). The orthogonal FL assay (Fig. 4b) and native-PAGE electrophoresis (Fig. S14†) showed good specific recognition. Then, the DMSN@H mixture was incubated with Hct116 cells in normal and hypoxic conditions. As expected, CLSM images with different distinct emission dots were obtained, indicating a successful GSH response and target miRNA-triggered self-assembly of amplifiers in living Hct116 cells (Fig. 4c and S15†). The decoded dots presented in Fig. S16† strongly demonstrated the ability to image multiplexed miRNAs. Compared with the cells in normal conditions, changes in the FL intensities of most of the amplifiers were observed in hypoxic conditions. The FL intensity assigned to miRNA-211, miRNA-346, and miRNA-210 separately increased 2.1, 2.65, 3.52 times, respectively, while the intensity for miRNA-153, miRNA-455, miRNA-141, miRNA-181 separately decreased by 3.2, 1.43, 1.29, 1.40 times, respectively. Only the miRNA-30c-2 had no statistically significant change. The FL intensity change trends were consistent with the quantitative reverse transcriptase polymerase chain reaction (qPCR) results (Fig. 4d) and previous reports.[26a,b,i,j,27] These results confirmed the robust performance of the designed multi-HCR for multiplexed miRNA profiling in developmental and pathological processes.

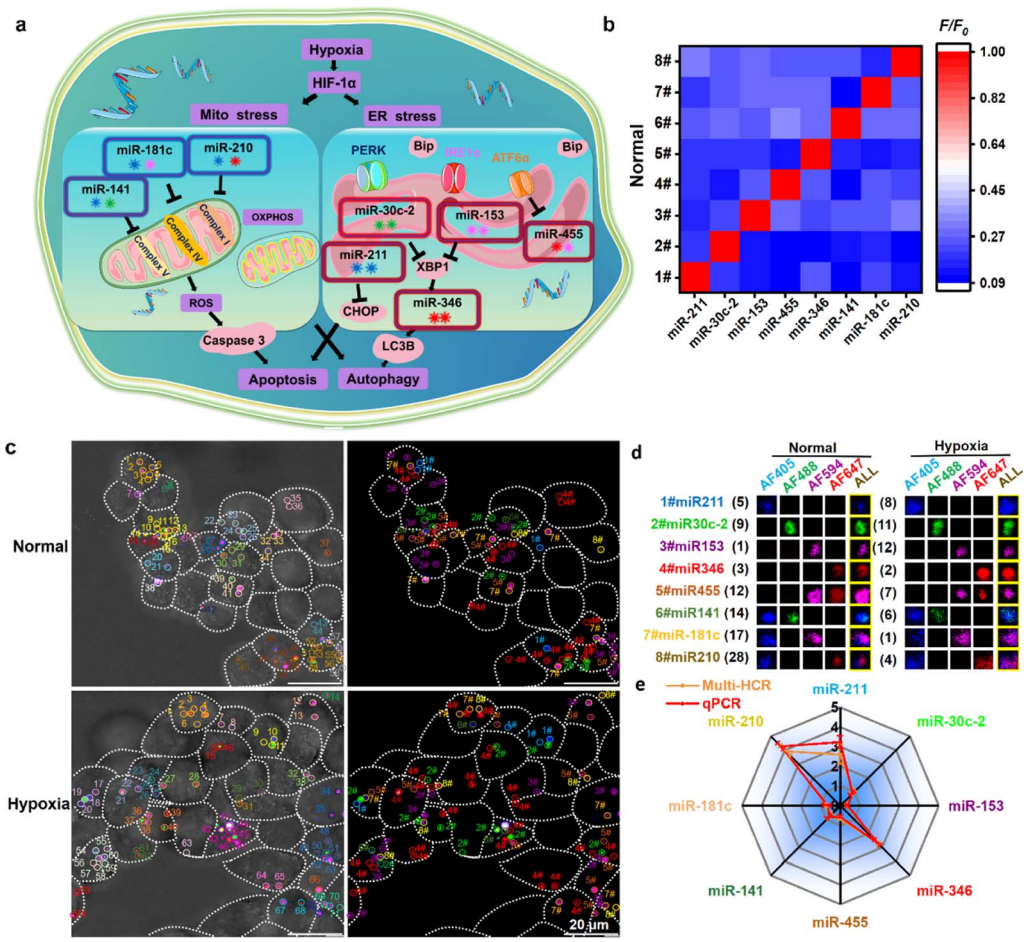

Fig. 4 Multiplexed miRNA profiling under hypoxia-induced Mito/ER stress and apoptosis/autophagy processes. (a) Schematic presentation of the hypoxia-induced miRNAs alteration. (b) Normalized heatmap for the specific test of the eight hypoxia-induced miRNAs. (c) Representative CLSM images for simultaneously profiling eight miRNAs using multi-HCR amplifiers. (d) Representative decoding and calculation process for the eight miRNAs in living cells (e) comparison of miRNA profiles tested by multi-HCR and qPCR methods. Each experiment was repeated three times.

Experimental

Synthesis of 80 nm biodegradable mesoporous silicon nanovector (DMSN)

The DMSN was synthesized using cetyltrimethylammoniumtosylate (CTAT) as a template and tetraethyl orthosilicate (TEOS) with bis[3-(triethoxysilyl)propyl] tetrasulfide (BTESPT) as biodegradable silica sources.[23b,28] 0.6 g of CTAT, 0.15 g of triethanolamine (TEA), and 40 mL of ddH_2O were stirred at 80 °C for 30 min. Then, a solution of 1.0 g of BTESPT and 4.0 g of TEOS was added dropwise to the solution. The resulting mixture was stirred at 1000 rpm at 70 °C for 2 h. The products were collected by centrifugation at 10 000 rpm for 20 min, washed with anhydrous ethanol, and refluxed in the anhydrous ethanol solution for 24 h. Finally, the DMSN was washed, collected, and dried for further use.

Synthesis of multi-HCR barcodes (DMSN@H)

The DMSN was modified with thiol groups (–SH) as follows:[29] 10 mg of DMSN was ultrasonically dispersed into 2 mL of anhydrous ethanol containing 0.03 g of CTAT, 0.008 g of TEA, 0.1 g of TEOS, and 0.1 g of METES. The mixture was stirred at 1000 rpm for 30 min at room temperature, then centrifuged and the sediment was washed three times using anhydrous ethanol. 10 μL of different HCR hairpins (100 μM) were separately mixed with 90 μL of Tris–HCl buffer (pH 7.4, 10 mM $MgCl_2$), and heated at 95 °C for 5 min, then kept at 37 °C for 2 h to stabilize the hairpin structure. 100 μL of DMSN-SH (10 mg mL^{-1}) was mixed with the above HCR hairpin buffer under gently shaken for 24 h at room temperature. Finally, the obtained DMSN@H was washed and resuspended in 1 mL of PBS buffer and kept at 4 °C for further use.

Multiplexed fluorescence assay in liquid solution

To assess the feasibility of detecting orthorhombic HCR hairpins assembled for 15 kinds of color compositions, different colors of hairpins were equally mixed at a total concentration of 120 nM and incubated with the target miRNA-155 (120 nM) at 37 °C for 4 h. For the specificity assay of the eight HCR hairpin pairs targeting eight kinds of miRNAs, 100 μL of total hairpins (120 nM) was incubated with 100 μL of targeting miRNAs (120 nM) at 37 °C for 4 h. The fluorescence intensity was measured on a Hitachi F-4500 fluorescence spectrometer (Tokyo, Japan). The AF405, AF488, AF595, and AF647 were excited at 402 nm, 488 nm, 594 nm, and 633 nm, and emissions peaks were recorded at 419 nm, 610 nm, and 665 nm, respectively.

Cell culture

For 0.2% O_2 incubation (hypoxia group), 1×10^4 Hct116 cells were cultured in an AnaerPack™-Anaero box (2.5 L). For 5% O_2 treatment, the cells were settled in an AnaerPack™-MicroAero (2.5 L). Other operations were similar to those in a normoxic environment (normal group).[30] All the cells were incubated in DMEM containing 10% FBS and 1% penicillin/streptomycin at 37 °C in a humidified atmosphere containing 5% CO_2.

CLSM imaging and analysis

Briefly, before incubating with the multi-HCR nanoparticles, 1×10^4 Hct116 cells were cultured under normal (21% O_2) and hypoxic (0.2% O_2) environments for 48 h. Then they were treated with the multi-HCR barcodes at a total concentration of 100 μg mL^{-1} (or 240 nM total HCR probes) per confocal dish of cells for 24 h at 37 °C under normal (21% O_2) and hypoxic (0.2% O_2) environments. The resulting cells were washed twice using PBS, and fresh DMEM (1 mL) was added. The scanning was in sequencing mode: AF405 was excited with a 405 nm laser line and detected with a 430–450 nm band-pass filter. AF488 was excited at 488 nm, with emission collected at 510–530 nm. AF594 and AF647 were excited with 561 nm and 633 nm lasers, respectively, then 590–620 nm and 650–700 nm filters were used for FL detection. Finally, the acquired FL barcodes were analyzed using ImageJ software (version 1.52i, USA), and a positive color composition was confirmed by subtracting three times the background fluorescence intensity.[23]

Statistical analysis

All of the results have been acquired by performing at least three independent experiments. All data are expressed in this manuscript as mean ± SD. A two-tailed Student's *t*-test was used to analyze the differences between the two groups. Asterisks indicate significant differences ($*p < 0.05$, $**p < 0.01$, $***p < 0.001$). The analysis was performed using Origin 2018 software (OriginLab Inc., USA).

Conclusions

Multiplexed *in situ* analysis of interacting molecules in living cells is of great importance for revealing cell physiopathology, clinical diagnostic applications, and biosensing. We report an encoded multi-HCR amplifier based on orthogonal amplification cascades with hybridization chain reactions. It comprises different colored metastable hairpins separately modified on mesoporous silica nanoparticles. After cellular uptake, the GSH-responsive hairpins are released and target miRNA-triggered orthogonal amplification, enabling self-assembly of 15 fluorescent HCR amplifiers for miRNA profiling. Excellent performance is achieved when imaging eight target miRNAs in hypoxia-induced Mito/ER stress and apoptosis and autophagy. The multi-HCR provides a robust tool for simultaneously profiling multiplexed biomarkers, facilitating a deeper understanding of interacting regulatory elements in developmental and pathological processes. It should be noted that connecting the barcoded nucleic acid chains with antibodies can easily extend the strategy to the high-throughput detection of protein biomarkers in living cells.

Author contributions

H. F. D. conceived the project and supervised all the experiments. Y. Y. Z. and Y. Y. W. did the electrophoresis experiments. W. W. and F. Y. performed FL analysis. S. S. Y. and J. Z. L. captured the TEM images. W. W and Y. F. Z did the qPCR

test. W. W. and L. P. Z performed cell culture and confocal microscopy analysis. H. F. D. and W. W. wrote the first edition of this manuscript.

Conflicts of interest

There are no conflicts to declare.

Acknowledgements

The work was supported by the Excellent Young Scientists Fund (22022407), Special Foundation for State Major Research Program of China (Grant 2022YFB3207202), Guangdong Province Pearl River Team (2021ZT09C289), Shenzhen Key Laboratory for Nano-Biosensing Technology (ZDSYS20210112161400001). 2021 Stability support plan of Shenzhen University (8940206/0200). We thank Instrumental Analysis Center of Shenzhen University for the assistance with the Electron Microscope/Nuclear Magnetic Resonance spectroscope/Mass Spectrometer/Confocal Microscope/Small Animal Diagnostics Imaging/Material Characterization technical support.

References

1 (*a*) X. Liu and Y.-T. Chang, *Chem. Soc. Rev.*, 2022, **51**, 1573–1591; (*b*) J. Shen, Y. Li, H. Gu, F. Xia and X. Zuo, *Chem. Rev.*, 2014, **114**, 7631–7677.

2 (*a*) T. Jet, G. Gines, Y. Rondelez and V. Taly, *Chem. Soc. Rev.*, 2021, **50**, 4141–4161; (*b*) Z. Xiang, J. Zhao, D. Yi, Z. Di and L. Li, *Angew. Chem.*, 2021, **60**, 22659–22663.

3 (*a*) E. Lubeck and L. Cai, *Nat. Methods*, 2012, **9**, 743–748; (*b*) R. Deng, K. Zhang, L. Wang, X. Ren, Y. Sun and J. Li, *Chem*, 2018, **4**, 1373–1386.

4 (*a*) M. Hill and N. Tran, *Trends Cancer*, 2018, **4**, 465–468; (*b*) H. Galagali and J. K. Kim, *Curr. Opin. Cell Biol.*, 2020, **67**, 118–140.

5 (*a*) T. Treiber, N. Treiber and G. Meister, *Nat. Rev. Mol. Cell Biol.*, 2019, **20**, 5–20; (*b*) S. Cai, T. Pataillot-Meakin, A. Shibakawa, R. Ren, C. L. Bevan, S. Ladame, A. P. Ivanov and J. B. Edel, *Nat. Commun.*, 2021, **12**, 3515.

6 (*a*) D. Wang, S. Li, Z. Zhao, X. Zhang and W. Tan, *Angew. Chem.*, 2021, **60**, 1–6; (*b*) T. Ueda, S. Volinia, H. Okumura, M. Shimizu, C. Taccioli, S. Rossi, H. Alder, C.-g. Liu, N. Oue, W. Yasui, K. Yoshida, H. Sasaki, S. Nomura, Y. Seto, M. Kaminishi, G. A. Calin and C. M. Croce, *Lancet Oncol.*, 2010, **11**, 136–146; (*c*) X.-H. Shi, X. Li, H. Zhang, R.-Z. He, Y. Zhao, M. Zhou, S.-T. Pan, C.-L. Zhao, Y.-C. Feng, M. Wang, X.-J. Guo and R.-Y. Qin, *Sci. Rep.*, 2018, **8**, 7638; (*d*) F. Kern, L. Krammes, K. Danz, C. Diener, T. Kehl, O. Küchler, T. Fehlmann, M. Kahraman, S. Rheinheimer, E. Aparicio-Puerta, S. Wagner, N. Ludwig, C. Backes, H.-P. Lenhof, H. von Briesen, M. Hart, A. Keller and E. Meese, *Nucleic Acids Res.*, 2020, **49**, 127–144; (*e*) B. Liu, B. Wang, X. Zhang, R. Lock, T. Nash and G. Vunjak-Novakovic, *Sci. Transl. Med.*, 2021, **13**, eabd0914.

7 J. B. Lawrence, R. H. Singer and L. M. Marselle, *Cell*, 1989, **57**, 493–502.

8 (*a*) S. S. Agasti, Y. Wang, F. Schueder, A. Sukumar, R. Jungmann and P. Yin, *Chem. Sci.*, 2017, **8**, 3080–3091; (*b*) P. Y. Weidong Xu and M. Dai, *Angew. Chem.*, 2018, **57**, 14075–14079.

9 E. Lubeck, A. F. Coskun, T. Zhiyentayev, M. Ahmad and L. Cai, *Nat. Methods*, 2014, **11**, 360–361.

10 J. J. L. Goh, N. Chou, W. Y. Seow, N. Ha, C. P. P. Cheng, Y.-C. Chang, Z. W. Zhao and K. H. Chen, *Nat. Methods*, 2020, **17**, 689–693.

11 (*a*) H. M. T. Choi, J. Y. Chang, L. A. Trinh, J. E. Padilla, S. E. Fraser and N. A. Pierce, *Nat. Biotechnol.*, 2010, **28**, 1208–1212; (*b*) M. Schwarzkopf and N. A. Pierce, *Nucleic Acids Res.*, 2016, **44**, e129; (*c*) H. M. T. Choi, V. A. Beck and N. A. Pierce, *ACS Nano*, 2014, **8**, 4284–4294.

12 J. Liu, T. Zheng and Y. Tian, *Angew. Chem.*, 2019, **58**, 7757–7761.

13 (*a*) F. Yang, Y. Cheng, Y. Cao, H. Dong, H. Lu, K. Zhang, X. Meng, C. Liu and X. Zhang, *Chem. Sci.*, 2019, **10**, 1709–1715; (*b*) Y. Cao, H. Dong, S. Pu and X. Zhang, *Nano Res.*, 2018, **11**, 4074–4081.

14 (*a*) M.-H. Kim, H.-K. Na, Y.-K. Kim, S.-R. Ryoo, H. S. Cho, K. E. Lee, H. Jeon, R. Ryoo and D.-H. Min, *ACS Nano*, 2011, **5**, 3568–3576; (*b*) P. Mora-Raimundo, D. Lozano, M. Benito, F. Mulero, M. Manzano and M. Vallet-Regí, *Adv. Sci.*, 2021, **8**, 2101107; (*c*) Y. Zhou, G. Quan, Q. Wu, X. Zhang, B. Niu, B. Wu, Y. Huang, X. Pan and C. Wu, *Acta Pharm. Sin. B*, 2018, **8**, 165–177.

15 C. Wang, H. Lin, X. Ge, J. Mu, L. Su, X. Zhang, M. Niu, H. Yang and J. Song, *Adv. Funct. Mater.*, 2021, **31**, 2009942.

16 (*a*) M. J. Lajoie, S. E. Boyken, A. I. Salter, J. Bruffey, A. Rajan, R. A. Langan, A. Olshefsky, V. Muhunthan, M. J. Bick, M. Gewe, A. Quijano-Rubio, J. Johnson, G. Lenz, A. Nguyen, S. Pun, C. E. Correnti, S. R. Riddell and D. Baker, *Science*, 2020, **369**, 1637–1643; (*b*) Q. Yang, J. Li, X. Wang, H. Xiong and L. Chen, *Anal. Chem.*, 2019, **91**, 6561–6568; (*c*) M. Xiao, K. Zou, L. Li, L. Wang, Y. Tian, C. Fan and H. Pei, *Angew. Chem., Int. Ed.*, 2019, **58**, 15448–15454.

17 (*a*) R. M. Dirks and N. A. Pierce, *Proc. Natl. Acad. Sci. U. S. A.*, 2004, **101**, 15275–15278; (*b*) Z. Wu, G.-Q. Liu, X.-L. Yang and J.-H. Jiang, *J. Am. Chem. Soc.*, 2015, **137**, 6829–6836.

18 Y. Li, Y. T. H. Cu and D. Luo, *Nat. Biotechnol.*, 2005, **23**, 885–889.

19 C. Hwang, A. J. Sinskey and H. F. Lodish, *Science*, 1992, **257**, 1496–1502.

20 R. Hong, G. Han, J. M. Fernández, B.-j. Kim, N. S. Forbes and V. M. Rotello, *J. Am. Chem. Soc.*, 2006, **128**, 1078–1079.

21 M. H. Lee, Z. Yang, C. W. Lim, Y. H. Lee, S. Dongbang, C. Kang and J. S. Kim, *Chem. Rev.*, 2013, **113**, 5071–5109.

22 (*a*) H. Sork, J. Z. Nordin, J. J. Turunen, O. P. B. Wiklander, B. Bestas, E. M. Zaghloul, H. Margus, K. Padari, A. D. Duru, G. Corso, J. Bost, P. Vader, M. Pooga, C. I. E. Smith, M. J. A. Wood, R. M. Schiffelers, M. Hällbrink and S. E. L. Andaloussi, *Mol. Ther.–Nucleic Acids*, 2016, **5**, e290; (*b*) H. Fang, Z. Guo, L. Lin, J. Chen, P. Sun, J. Wu, C. Xu, H. Tian and X. Chen, *J. Am. Chem. Soc.*, 2018, **140**, 11992–12000; (*c*) K. Ren, Y. Liu, J. Wu,

Y. Zhang, J. Zhu, M. Yang and H. Ju, *Nat. Commun.*, 2016, **7**, 13580; (*d*) W. Wei, W. Dai, F. Yang, H. Lu, K. Zhang, Y. Xing, X. Meng, L. Zhou, Y. Zhang, Q. Yang, Y. Cheng and H. Dong, *Angew. Chem.*, 2022, **61**, e202116909.

23 (*a*) W. Wei, W. Cheng, W. Dai, F. Lu, Y. Cheng, T. Jiang, Z. Ren, Y. Xie, J. Xu, Q. Zhao, X. Yu, Y. Yin, J. Li and H. Dong, *Nano Lett.*, 2022, **22**, 211–219; (*b*) D. Shao, M. Li, Z. Wang, X. Zheng, Y. H. Lao, Z. Chang, F. Zhang, M. Lu, J. Yue, H. Hu, H. Yan, L. Chen, W. F. Dong and K. W. Leong, *Adv. Mater.*, 2018, **30**, e1801198; (*c*) N. Yan, L. Lin, C. Xu, H. Tian and X. Chen, *Small*, 2019, **15**, e1903016.

24 (*a*) K. Jiao, Q. Yan, L. Guo, Z. Qu, S. Cao, X. Chen, Q. Li, Y. Zhu, J. Li, L. Wang, C. Fan and F. Wang, *Angew. Chem.*, 2021, **60**, 14438–14445; (*b*) S. Zhu, H. Xing, P. Gordiichuk, J. Park and C. A. Mirkin, *Adv. Mater.*, 2018, **30**, 1707113; (*c*) M. K. Vasher, G. Yamankurt and C. A. Mirkin, *J. Am. Chem. Soc.*, 2022, **144**, 3174–3181; (*d*) S. B. Ebrahimi, D. Samanta and C. A. Mirkin, *J. Am. Chem. Soc.*, 2020, **142**, 11343–11356.

25 M. E. Crosby, R. Kulshreshtha, M. Ivan and P. M. Glazer, *Cancer Res.*, 2009, **69**, 1221–1229.

26 (*a*) F. Elena, R. Anassuya, M. C. Robert, G. Harriet, B. Christine, C. Meredith, D. Cecilia, B. Christopher, B. Francesca and J. L. Li, *PLoS One*, 2010, **5**, e10345; (*b*) D. Sabry, S. E. M. El-Deek, M. Maher, M. A. H. El-Baz, H. M. El-Bader, E. Amer, E. A. Hassan, W. Fathy and H. E. M. El-Deek, *Mol. Cell. Biochem.*, 2019, **454**, 177–189; (*c*) Z. Chen, Y. Li, H. Zhang, P. Huang and R. Luthra, *Oncogene*, 2010, **29**, 4362–4368; (*d*) J. Guo, Z. Yang, X. Yang, T. Li, M. Liu and H. Tang, *Cancer Lett.*, 2018, **413**, 69–81; (*e*) R. Bartoszewski, J. W. Brewer, A. Rab, D. K. Crossman, S. Bartoszewska, N. Kapoor, C. Fuller, J. F. Collawn and Z. Bebok, *J. Biol. Chem.*, 2011, **286**, 41862–41870; (*f*) S. Das, M. Kohr, B. Dunkerly-Eyring, D. I. Lee, D. Bedja, O. A. Kent, A. K. Leung, J. Henao-Mejia, R. A. Flavell and C. Steenbergen, *J. Am. Heart Assoc.*, 2017, **6**, e004694; (*g*) W. A. Baseler, D. Thapa, R. Jagannathan, E. R. Dabkowski, T. L. Croston and J. M. Hollander, *Am. J. Physiol.: Cell Physiol.*, 2012, **303**, C1244–C1251; (*h*) S. Jiang, L.-F. Zhang, H.-W. Zhang, S. Hu, M.-H. Lu, S. Liang, B. Li, Y. Li, D. Li, E.-D. Wang and M.-F. Liu, *EMBO J.*, 2012, **31**, 1985–1998; (*i*) G. Wan, W. Xie, Z. Liu, W. Xu, Y. Lao, N. Huang, K. Cui, M. Liao, J. He and Y. Jiang, *Autophagy*, 2014, **10**, 70–79; (*j*) N. S. Chitnis, D. Pytel, E. Bobrovnikova-Marjon, D. Pant, H. Zheng, N. L. Maas, B. Frederick, J. A. Kushner, L. A. Chodosh, C. Koumenis, S. Y. Fuchs and J. A. Diehl, *Mol. Cell*, 2012, **48**, 353–364; (*k*) A. E. Byrd, I. V. Aragon and J. W. Brewer, *J. Cell Biol.*, 2012, **196**, 689–698; (*l*) H. Liang, J. Xiao, Z. Zhou, J. Wu, F. Ge, Z. Li, H. Zhang, J. Sun, F. Li, R. Liu and C. Chen, *Oncogene*, 2018, **37**, 1961–1975; (*m*) P. J. Belmont, W. J. Chen, D. J. Thuerauf and C. C. Glembotski, *J. Mol. Cell. Cardiol.*, 2012, **52**, 1176–1182.

27 (*a*) R. Kulshreshtha, M. Ferracin, S. E. Wojcik, R. Garzon, H. Alder, F. J. Agosto-Perez, R. Davuluri, C.-G. Liu, C. M. Croce, M. Negrini, G. A. Calin and M. Ivan, *Cell. Mol. Biol.*, 2007, **27**, 1859–1867; (*b*) Y.-M. Meng, X. Jiang, X. Zhao, Q. Meng, S. Wu, Y. Chen, X. Kong, X. Qiu, L. Su, C. Huang, M. Wang, C. Liu and P.-P. Wong, *Nat. Commun.*, 2021, **12**, 6011; (*c*) W. Li, J. Yang, L. Luo, M. Jiang, B. Qin, H. Yin, C. Zhu, X. Yuan, J. Zhang, Z. Luo, Y. Du, Q. Li, Y. Lou, Y. Qiu and J. You, *Nat. Commun.*, 2019, **10**, 3349.

28 Y. Xing, Q. Pan, X. Du, T. Xu, Y. He and X. Zhang, *ACS Appl. Mater. Interfaces*, 2019, **11**, 10426–10433.

29 K. Zhang, X. Meng, Z. Yang, Y. Cao, Y. Cheng, D. Wang, H. Lu, Z. Shi, H. Dong and X. Zhang, *Adv. Mater.*, 2019, **31**, e1807888.

30 K. Zhang, Z. Yu, X. Meng, W. Zhao, Z. Shi, Z. Yang, H. Dong and X. Zhang, *Adv. Sci.*, 2019, **6**, 1900530.